CGU HS Committee on River Ice Processes and the Environment
19th Workshop on the Hydraulics of Ice Covered Rivers
Whitehorse, Yukon, Canada, July 9-12, 2017.

The River Ice Automated Classifier Tool (RIACT)

Thomas Puestow[1], Andrew Cuff[1], Martin Richard[2], Simon Tolszczuk-Leclerc[3], Jean-Samuel Proulx-Bourque[3], Alice Deschamps[3], Joost van der Sanden[3] and Sherry Warren[1]

[1]*C-CORE, Capt. Robert A. Bartlett Building, Morrissey Road, St. John's, NL, A1B 3X5, Canada*
thomas.puestow@c-core.ca; andrew.cuff@c-core.ca; sherry.warren@c-core.ca

[2]*National Research Council Canada, Ice Mechanics / Ocean, Coastal and River Engineering*
martin.richard@nrc-cnrc.gc.ca

[3]*Natural Resources Canada, 560 Rochester Street, Ottawa, ON, K1S 5K2, Canada*
simon.tolszczuk-leclerc@canada.ca; jean-samuel.proulx-bourque@canada.ca; alice.deschamps@canada.ca; joost.vandersanden@canada.ca

This investigation was carried out to improve the identification of potential ice jams using satellite imagery for Natural Resources Canada's Emergency Geomatics Services (EGS) group. The study site comprised the Athabasca River around the town of Fort McMurray during the breakup period. Satellite imagery used included RADARSAT-2 Fine and Standard Beam data collected in 2014 and 2015. Field observations for algorithm training and validation were supplied by Alberta Environment and Parks in the form of river ice observation reports and aerial photography. Predictor variables for input to the classification included speckle-filtered HH and HV backscatter, grey level co-occurrence matrix (GLCM) mean and entropy texture measures, and incidence angles. Dedicated datasets for classifier training and validation were collected throughout the study areas. The classification of river ice types was carried out using decision tree analysis (DTA), with separate decision trees developed for different combinations of predictor variables. The best result, with an overall accuracy of 95%, was obtained if backscatter, texture and incidence angle information were used in concert. The fully automated execution, the ability to generate products from imagery acquired at low incidence angles and the observed classification accuracy indicate significant operational potential for the RIACT algorithm.

1. Introduction

Floods account for the greatest number of hydrological and meteorological natural disaster events in Canada, and for most Canadian rivers the annual peak water levels are due to ice jams (Thistlethwaite and Feltmate, 2013; Government of Canada 2009). The formation and decay of river ice covers is a highly complex process controlled largely by flow characteristics, temperature and precipitation (Weber et al., 2003). The severity and economic impact of floods related to ice jams is exacerbated by the danger of post-flooding freeze-up.

Key parameters required to assess the danger of flooding due to ice jams include location, extent and structure of the ice field. However, a systematic determination of these parameters is difficult to achieve over large areas using conventional, field-based and aerial surveillance methods (Beltaos and Burrell, 2015). In remote and inaccessible areas, frequent surveillance can be cost prohibitive. Under these conditions, Earth Observation (EO) has emerged as a promising tool to collect information on river ice development over large areas repeatedly and consistently throughout the ice season. Satellite Synthetic Aperture Radar (SAR) imagery in particular has been shown to yield cost-effective information regarding ice type on medium and large rivers within an operational context (Weber et al., 2003; Tracy and Daly, 2003; Pelletier et al., 2003; Puestow et al., 2004; Pelletier et al., 2005; Mermoz et al., 2009; Khan and Puestow, 2010; Gauthier et al., 2010; Jasek et al., 2013; Gauthier et al., 2015; Khan and Puestow, 2015; Deschamps et al., 2015).

The radar response of river ice covers is dominated by surface and volume scattering (Pelletier et al., 2005; Unterschultz et al., 2009; Gherboudj et al., 2010). Surface scatter is a result of the interaction between the radar signal and an interface at which there is a change in dielectric constant. Smooth surfaces usually result in specular reflection, directing most of the energy away from the sensor in a single direction. Rough surfaces, on the other hand, tend to cause diffuse scattering, reflecting the energy nearly uniformly in all directions and directing more radiation back toward the sensor. Rougher surfaces therefore tend to generate a greater amount of surface scatter.

In the case of volume scattering, the radiation penetrates into the ice cover and the radar signal is scattered by dielectric discontinuities within the medium, such as air bubbles, liquid water pockets and particles. Inhomogeneous ice covers typically show larger backscatter coefficients than more uniform ice covers. Volume scattering requires the ice to be dry with little liquid water content. If the ice is wet, surface scattering is the dominant scattering mechanism.

C-CORE has been providing satellite-based river ice monitoring services since 2004 for rivers in Canada, the United States and Russia (Puestow et al., 2004; Pryse-Phillips et al., 2009; Khan and Puestow 2010; Khan and Puestow 2015). Emphasizing operational monitoring and the provision of tactical information in near real-time (NRT), the generation of ice information products relies on a semi-automated analysis framework that integrates satellite and in-situ observations (C-CORE, 2012). This process is applied throughout the ice season from ice formation to breakup.

Russell et al., (2009) demonstrated the utility of HH-HV dual-pol SAR imagery in automated river ice classification. Using ENVISAT imagery collected from 2005-2008, study areas included the Athabasca, Saint John, Exploits Rivers in Canada, as well as the Yenisei River in Russia. Field data included annotated maps, aerial and field photographs, aerial video and ice observer reports.

EO data and field data were correlated by date and location to identify suitable training sites. A quadratic discriminant classifier algorithm was developed based on image backscatter values and texture measures derived from the Grey Level Co-occurrence Matrix (GLCM). A sequential forward selection algorithm was employed to reduce the set of variables used in the classification. The results indicate the potential for improved ice class separability by incorporating both the HV channel and GLCM texture measures, confirming the utility of dual polarized SAR imagery for improved ice type discrimination.

Van der Sanden and Deschamps (2014) and Deschamps et al., (2015) describe an automated satellite-based approach for the classification of breaking river ice cover implemented as the Ice Breakup Classification (IceBC). Exploiting the sensitivity of SAR to differences in the roughness of river ice covers during breakup, the process uses C-band SAR, HH single-pol images as input. In order to increase the discrimination of ice and water, only incidence angles greater than 36° are considered. The algorithm returns the principal classes of sheet ice (smooth textures), rubble ice (rough textures) and water, whereby three sub-categories are defined for both sheet and rubble ice. Although the process is largely automated, additional interpretation by subject matter experts is required to resolve potential ambiguities (e.g., similar SAR signatures for moving and stationary ice, presence of water or wet snow on ice).

This study was carried out within a larger project aiming to develop improved tools for flood hazard assessment by the Emergency Geomatics Service (EGS) group of Natural Resources Canada (NRCan). It was the goal of this research to improve the identification of potential ice jams using satellite imagery. With an emphasis on the Athabasca River around the town of Fort McMurray during the breakup period, the investigation aimed to address the following objectives:

- Evaluate the contribution of the cross-pol channel (i.e. HV) to river ice classification;
- Evaluate the contribution texture information to river ice classification;
- Emphasize the separation of ice and water; and
- Implement an automated classification tool compatible with EGS processes.

2. Methods

This investigation focused on the Athabasca River around Fort McMurray as presented in Figure 1. Originating from the Columbia Ice Field in the Rocky Mountains, the Athabasca River flows more than 1200 km north-east to drain into the Peace-Athabasca Delta. Ice-related flooding is a recurring concern for Fort McMurray, a major regional administrative and industrial center with population of approximately 80,000. An active aerial ice surveillance program is conducted during the spring breakup period by Alberta Environment and Parks to monitor ice conditions and assess flood risk.

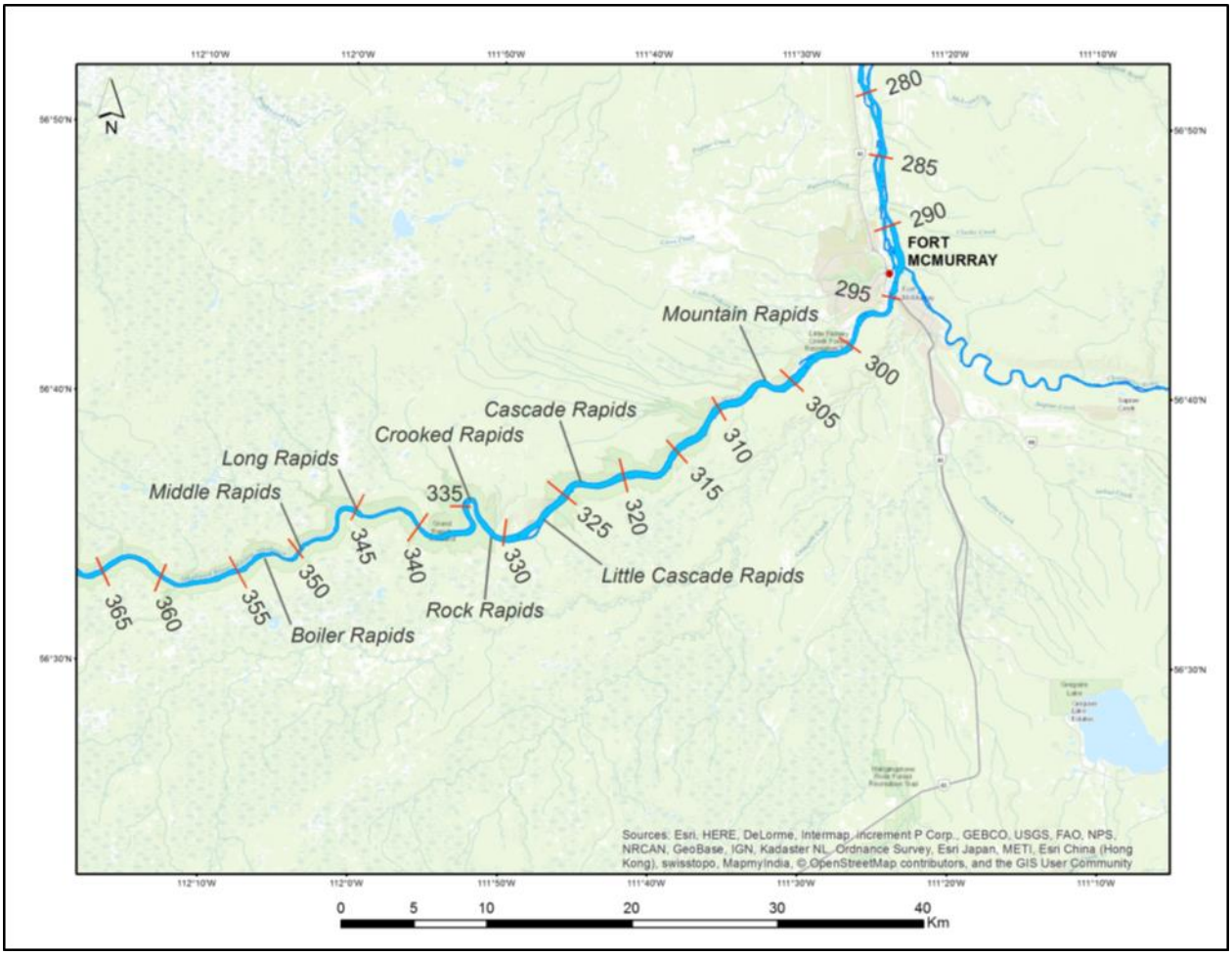

Figure 1. Study area with numbered river sections (descending in downstream direction)

This study used RADARSAT-2 satellite SAR imagery collected in 2014 and 2015 as presented in Table 1. All satellite data had been previously collected and made available to the project by NRCan. All images used were acquired during the spring breakup phase. In addition, air temperature and wind speed observations coinciding with the satellite image acquisition were provided by NRCan.

Table 1. Characteristics of RADARSAT-2 imagery used in the study

Beam Mode	Incidence Angle [^{o}]	Polarization	Acquisition Date	Orbit	Local Time
Standard 8	48.5 – 52.1	HH, HV	April 17, 2014	Ascending	18:29
Standard 7	44.4 – 49.3	HH, HV	April 17, 2014	Descending	06:33
Wide Fine Quad-Pol 16	34.8 – 37.6	HH, HV, VH, VV	April 20, 2014	Descending	06:46
Wide Fine Quad-Pol 20	38.6 – 41.3	HH, HV, VH, VV	April 21, 2014	Ascending	18:12
Wide Fine Quad-Pol 5	22.5 – 26.0	HH, HV, VH, VV	April 23, 2014	Descending	06:58
Wide Fine Quad-Pol 5	22.5 – 26.0	HH, HV, VH, VV	April 25, 2014	Ascending	17:56
Wide Standard Quad-Pol 5	38.6 – 41.3	HH, HV, VH, VV	April 27, 2014	Descending	06:42
Wide Standard Quad-Pol 20	38.6 – 41.3	HH, HV, VH, VV	April 16, 2015	Ascending	18:46

A water mask created from LANDSAT imagery and provided by NRCan was used to ensure all land areas were removed from the analysis. The water mask was overlaid on the SAR imagery and manually corrected for geometric errors where necessary.

Field observations for algorithm training and validation were supplied by Alberta Environment and Parks in the form of river ice observation reports and aerial photography. River ice observation reports and maps were retrieved from the Alberta Environment and Parks archive of river ice observations (http://www.environment.alberta.ca/forecasting/RiverIce/). The difference between in-situ and satellite observations ranged from 3 to 8.5 hours.

This investigation focused on the use of dual-pol SAR imagery, specifically the HH co-pol and HV cross-pol channels. Accordingly, only HH and HV magnitude information was extracted from fully polarimetric RADARSAT-2 imagery as required. In alignment with the IceBC algorithm, HH and HV backscatter was expressed as gamma nought ($\gamma 0$) (van der Sanden and Deschamps, 2014).

The images were orthorectified using the rational function models and polynomial coefficients supplied with the RADARSAT-2 imagery (MDA, 2016). The pixel spacing selected for Fine and Standard Beam data was 6.5 and 12.5 meters, respectively. Nearest neighbour resampling was carried out to define pixel values in the orthorectified imagery. The HH and HV backscatter images were subjected to speckle reduction using gamma maximum a-posteriori filtering (Lopes et al., 1993). Following the IceBC pre-processing routines, speckle filtering was carried out in two stages using varying window sizes and effective number of looks. The speckle-filtered backscatter were subsequently converted from power to dB values.

Predictor variables for input to the classification included speckle-filtered HH and HV backscatter ($\gamma 0$), image texture and incidence angles.

Describing the spatial variability of brightness features among neighboring pixels, image texture has been used to capture spatial information contained in images (Haralick and Shanmugam 1973). A commonly used approach to extract image texture is based on the GLCM. The GLCM is a two-dimensional (2D) histogram, which evaluates pairs of pixels separated by a given distance across a defined direction. Each entry in the matrix corresponds to the frequencies of occurrence of grey

level combinations of pairs of pixels (Haralick et al., 1973; Soh and Tsatsoulis, 1999). Texture measures based on the GLCM can be broadly grouped into categories relating to contrast, orderliness and descriptive statistics. The texture measures GLCM mean and GLCM entropy were used in this investigation based on their documented performance in discriminating between river ice classes (Gauthier et al., 2006; Russell et al., 2009).

Incidence angle is a key factor affecting SAR backscatter, whereby similar surfaces show different backscatter signatures at different incidence angles. The impact of incidence angle variation can be minimized by selecting images acquired with similar incidence angles. However, this generally requires that image acquisitions are spaced one repeat cycle apart, which in the case of RADARSAT-2 is 24 days. For applications such as river ice monitoring, this is not practical as a much higher frequency of temporal coverage is required to capture dynamic ice cover changes. Therefore, river ice monitoring relies on the use of imagery acquired at different incidence angles. The use of image texture mitigates the impact of incidence angles on backscatter to some degree, as texture measures are based on spatial variation of brightness values within a defined neighbourhood of pixels. In addition, this investigation used incidence angle as explicit predictor variable in an effort to minimize unexplained variance in river ice classes. To this end, the incidence angle information contained in the RADARSAT-2 metadata was used to generate image channels containing the nominal incidence angle for each pixel.

Samples for use in classifier training and validation were collected as contiguous groups of pixels (polygons) located throughout the area of interest (Chen and Stow, 2002). In selecting an appropriate size for training and validation polygons, visual interpretation of the RADARSAT-2 and airborne imagery was carried out to identify the dimensions of small river ice features discernable in both satellite and aerial observations.

Nominally square sampling polygons were defined with a side length of 100 meters, resulting in polygon sizes of 8 x 8 and 16 x 16 pixels for fine and standard beam imagery, respectively. A random sampling scheme was implemented to locate the initial centroid locations for training polygons. In order to maximize the probability that pixels in neighboring polygons are independent from each other, the distance between polygon centroids was selected to be at least 200 meters. The actual shape of training and validation polygons was adjusted locally, where required, to ensure the collection of pixels over homogeneous areas.

The location of river sections used to select training and validation data was primarily based on areas covered by aerial photographs. In some cases, polygons were defined in areas located beyond the actual air photo coverage based on readily interpretable radar signatures and ice surveillance reports (e.g. open water and ice jam). Polygons containing training and validation data were initially captured as vectors (i.e. shape file format) and subsequently converted to a bitmap mask for the extraction of the corresponding pixel values for each predictor variable. Each polygon was assigned one of the following ice classes:

- Open water
- Sheet ice (labelled intact ice in field reports)
- Rubble ice (labelled ice jams in field reports)

Using the method described above, a total of 663 polygons were collected. The polygons were randomly divided into training data (413 polygons, 61938 pixels) and validation data (176 polygons, 26924 pixels). The following information was recorded for each pixel in each polygon:

- Unique polygon ID
- Ice type
- Unfiltered HH and HV backscatter
- Speckle-filtered HH and HV backscatter
- HH and HV GLCM Mean and Entropy
- HH and HV GLCM Entropy
- Incidence angle
- Date and time of image acquisition
- Time difference between image acquisition and field visits

The classification of river ice types was carried out using a decision tree analysis (DTA). DTA allows the formulation of relationships between one response (i.e. dependent) variable and several predictor (i.e. independent) variables by dividing a data set recursively into smaller, increasingly homogeneous portions. The final result constitutes a division of the original data set into mutually exclusive and exhaustive sub-sets (Morgan and Sonquist, 1963; Kass, 1980; Breiman et al., 1984; Quinlan et al., 1987; Biggs et al., 1991).

Performed for either exploratory analysis or predictive modelling, DTA requires no limiting assumptions about data distributions, it allows the simultaneous handling of categorical and continuous variables in the same data set, and permits the detection of non-linear interactions between variables (Lees and Ritman, 1991); Fabricius and Coetzee, 1992); Dymond and Luckman, 1994; Costanza and Paccaud, 2004; Chang and Chen, 2005; Crall et al., 2006). These properties make DTA ideally suited to problems with limited or no a-priori knowledge about the distribution and interaction of parameters in question.

DTA was carried out using the method described by Breiman et al. (1984), implemented as recursive partitioning (rpart) in the R statistical computing environment (Therneau and Atkinson, 2015). The rpart procedure was executed through the Rattle graphical user interface, Version 4.1.3 (Williams, 2009). At every level of the tree, stepwise splitting is performed by examining each of the predictor variables in turn and selecting the predictor resulting in the largest reduction in impurity as measured by the Gini index. Separate decision trees were developed for the following combinations of predictor variables:

- Scenario 1: HH backscatter;
- Scenario 2: HH and HV backscatter;
- Scenario 3: HH and HV backscatter, GLCM Mean and GLCM Entropy; and
- Scenario 4: HH and HV backscatter, GLCM Mean and GLCM Entropy, incidence angle.

For each scenario, an initial decision tree with a large number (i.e., hundreds) of terminal nodes was grown. Parameters reported for each split in the initial tree included complexity (*cp*), relative error as evaluated by the training sample, classification error as evaluated by a 10-fold cross-validation (*xerror*), and standard error of the cross-validation risk (*xstd*). In order to reduce the

likelihood of overfitting, redundant splits were removed from the initial trees using the *xerror* and *cp* parameters in a process called pruning. To this end, the minimum value of *xerror* was identified together with the complexity parameter corresponding to *xerror + xstd*. The tree was subsequently re-grown with the resulting *cp* value. The terminal nodes of each decision tree were interpreted as classification rules in the form of conditional "IF…THEN…" statements. An example of classification rules derived from DTA and expressed in pseudo-code is presented as follows:

IF HH < -20.14 dB THEN Class = Water
IF HH >= -20.14 dB and HH < -19.37 dB THEN Class = Water
IF HH < -18.94 dB and HH >= -19.37 dB THEN Class = Sheet Ice
IF HH < -11.42 dB and HH >= -18.94 THEN Class = Sheet Ice
IF HH >= -11.42 dB and HH < -9.902 dB THEN Class = Sheet Ice
IF HH >=-9.902 dB THEN Class = Rubble Ice

All pre-processing and classification procedures were implemented as a series of python scripts to be executed within PCI Geomatica 2015. The classification accuracy was assessed using the validation dataset. Confusion matrices were used to estimate overall accuracy as well as omission and commission errors (Congalton and Green. 1993).

3. Results

For each classification scenario described in Section 2, a separate set of classification rules was implemented and evaluated. The corresponding confusion matrices are presented in Table 2 to Table 5. Each table summarizes the number of pixels classified as a particular category (rows) versus the actual ice type as observed in the validation data set (columns).

Table 2. Classification result – Scenario 1 (HH only)

Accuracy: 79.7%	**Reference**				
Classification		**Water**	**Sheet Ice**	**Rubble Ice**	**Total**
	Water	1951	1023	38	**3012**
	Sheet Ice	1077	14656	1815	**17548**
	Rubble Ice	20	1485	4859	**6364**
	Total	**3048**	**17164**	**6712**	**26924**

Table 3. Classification result – Scenario 2 (HH, HV)

Accuracy: 84.0%	**Reference**				
Classification		**Water**	**Sheet Ice**	**Rubble Ice**	**Total**
	Water	1823	530	31	**2384**
	Sheet Ice	1208	15093	968	**17269**
	Rubble Ice	17	1541	5713	**7271**
	Total	**3048**	**17164**	**6712**	**26924**

Table 4. Classification result – Scenario 3 (HH, HV, Texture)

Accuracy: 86.5%	**Reference**				
Classification		**Water**	**Sheet Ice**	**Rubble Ice**	**Total**
	Water	2229	472	0	**2701**
	Sheet Ice	819	15212	862	**16893**
	Rubble Ice	0	1480	5850	**7330**
	Total	**3048**	**17164**	**6712**	**26924**

Table 5. Classification result – Scenario 4 (HH, HV, Texture, Incidence Angle)

Accuracy: 94.5%	**Reference**				
Classification		**Water**	**Sheet Ice**	**Rubble Ice**	**Total**
	Water	2612	311	0	**2923**
	Sheet Ice	430	16585	455	**17470**
	Rubble Ice	6	268	6257	**6531**
	Total	**3048**	**17164**	**6712**	**26924**

The overall accuracy is increasing with an increasing number of predictor variables. Using the HH backscatter only, an overall accuracy of 79.7% was achieved, which most of the error related to the misclassification of water and sheet ice, as well as sheet ice and rubble ice. Adding HV backscatter information increased the overall accuracy to 84%. In this case, the classification error was primarily due to the confusion between water and sheet ice. The classification accuracy increased incrementally to 86.5% with the addition of GLCM mean and entropy texture measures. The largest improvement in this case is related to the differentiation of sheet ice and water. The highest accuracy was achieved using all predictor variables in the classification, i.e. HH and HV backscatter, texture measures and incidence angle. In this case, an overall classification accuracy of 94.5% was observed. The largest classification error was associated with the category water, with omission and commission errors of 14.3% and 10.6% respectively. The corresponding errors for the sheet and rubble ice classes ranged from 3.4% to 6.8%.

The classification rules corresponding to Scenario 4 were implemented together with all relevant pre-processing procedures as the River Ice Automated Classification Tool (RIACT). The performance of the RIACT algorithm was qualitatively compared to the IceBC algorithm applied to the same RADARSAT-2 scenes. Figure 2 and Figure 3 show examples for Fine and Standard quad-pol imagery, together with relevant sections of aerial surveillance data. In the RIACT, water is displayed in blue, sheet ice in yellow and rubble ice in red. In the IceBC products, water is indicated as dark and light blue, sheet ice as green and yellow, and rubble ice as orange and red. The example in Figure 6 shows a river section largely classified as sheet ice in RIACT, with several locations of open water. While generally similar, the IceBC product generated for the same area shows more open water. The sheet ice cover is characterized by different stages of deterioration.

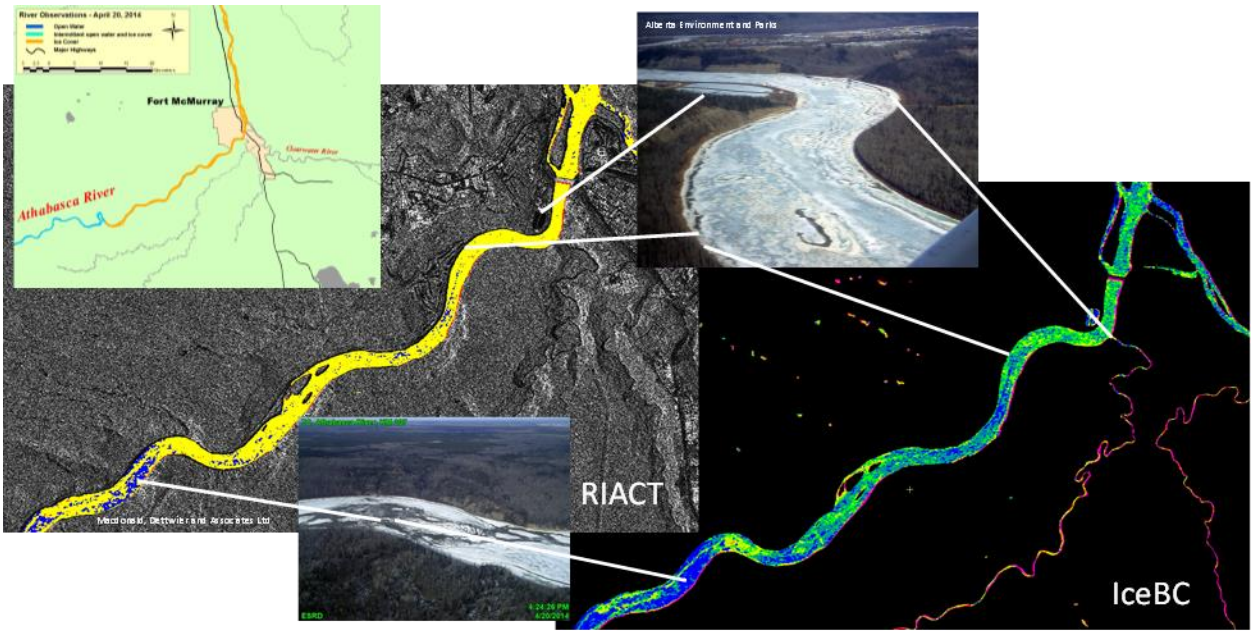

Figure 2. Comparison of RIACT and IceBC results - April 21 (Wide Fine Quad-Pol 20)

By contrast, the example in Figure 3, acquired several days later in the breakup phase, shows close correspondence of the RIACT and IceBC outputs.

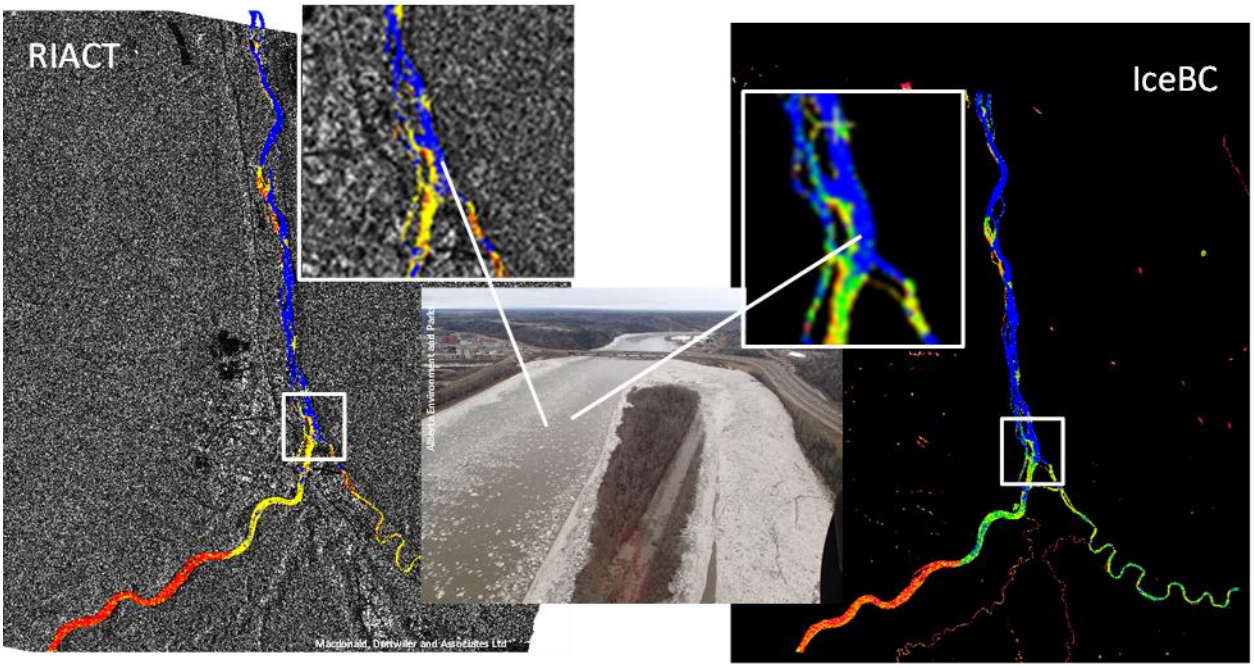

Figure 3. Comparison of RIACT and IceBC results - April 27 (Wide Standard Quad-Pol 20)

In this case, the different classes are well defined, with a stationary ice jam, intact sheet ice and ice-free open water. A major difference between RIACT and IceBC is the ability of the former to

generate products at low incidence angles. An example is presented in Figure 4, showing good correspondence with the available aerial imagery and field reports.

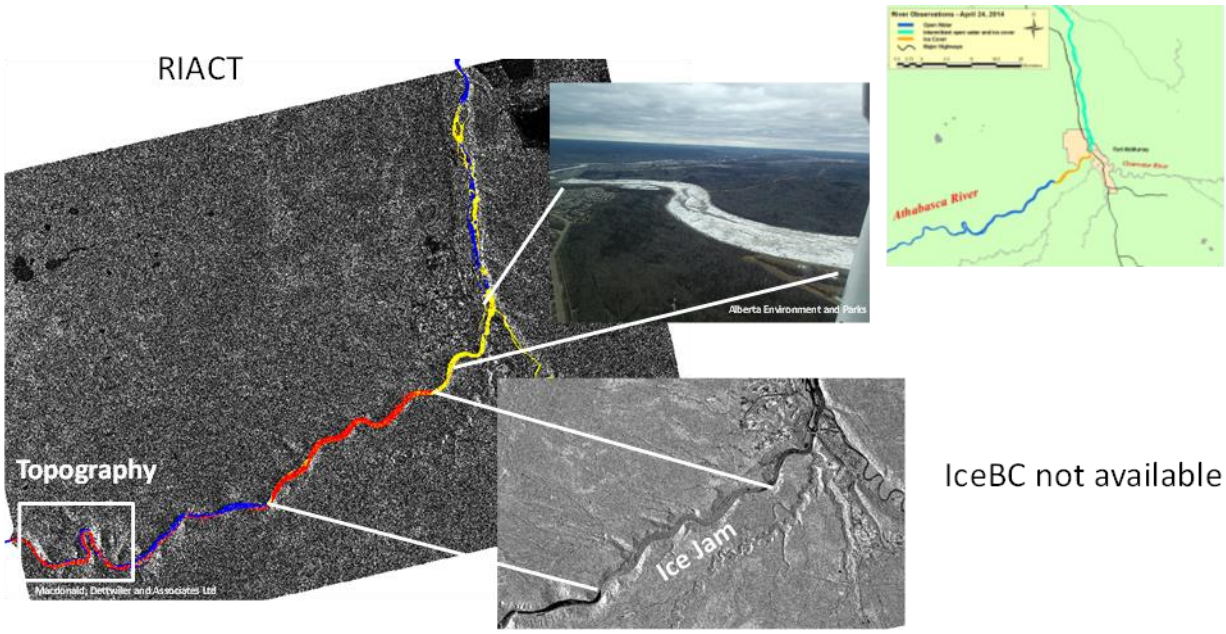

Figure 4. RIACT product generated for low incidence angle - April 25 (Wide Fine Quad-Pol 5)

Using only HH backscatter as a predictor variable, the RIACT algorithm achieved an overall classification accuracy of nearly 80%. This figure is largely due to the correct classification of pixels belonging to the sheet ice class, with associated commission and omission errors of 16% and 15%, respectively. The corresponding errors for the categories water and rubble ice were much higher, ranging from 28% to 36%. In consequence, using HH backscatter only within RIACT is not considered a viable option for operational implementation, as operational information needs emphasize the correct differentiation between ice and water, as well as the delineation of rubble ice as an indicator of potential ice jams.

Adding the cross-pol channel as a second predictor variable increased the overall classification accuracy to 84%. However, while an accuracy of nearly 90% is observed for sheet ice, the accuracies associated with water and rubble ice remain low, with classification errors ranging from 21% to 40%. The inclusion of the texture measures GLCM mean and GLCM entropy caused a modest increase in overall accuracy to 86.5%. The most notable improvement was observed for the category water, with omission and commission errors of 27% and 17%, respectively. However, the overall performance is still not considered adequate for operational needs.

By contrast, including incidence angle information in the classification process resulted in a marked increase in overall accuracy and decrease in classification errors (3% to 14%). As a result, RIACT shows significant operational potential. Of particular interest is the ability of RIACT to generate products at low incidence angles. This is in contrast to currently operational procedures that do not process imagery acquired at incidence angles of less than 35^0 due to the increasing similarity of ice and water at these angles (C-CORE, 2012; Deschamps et al., 2015).

The qualitative comparison with IceBC shows generally good agreement for the major ice categories. In some cases, RIACT appears to underestimate areas covered by water compared to IceBC output. This is particularly evident in images acquired early in the breakup period and is likely linked to sheet ice cover in various stages of deterioration. Conversely, IceBC is not currently able to generate products from imagery acquired at low incidence angles, whereas RIACT can generate products at all incidence angle ranges under investigation.

4. Conclusion and Recommendations

This investigation successfully developed, implemented and validated a fully automated process chain for satellite-based river ice classification. The underlying classification rules were derived using decision tree analysis. Using both RADARSAT-2 Fine and Standard Beam imagery, separate classification scenarios evaluated the utility of HH and HV backscatter, image texture and incidence angle as predictor variables. The best result with an overall accuracy of 95% was obtained when all predictors were used in the classification process.

The fully automated execution, the ability to generate products from imagery acquired at low incidence angles and the observed classification accuracy indicate significant operational potential for the RIACT algorithm. However, the algorithm has been trained and validated for one particular location and ice regime. In order to apply RIACT to other rivers across Canada, it will likely be necessary to retrain the algorithm using location-specific satellite and in-situ observations. The separation of ice and water remains challenging, indicating that other variables may need to be included to capture decaying ice covers more accurately. For example physical environmental variables such as air temperature, wind speed and precipitation are readily available and could easily be included in a tree-based classification approach.

This investigation used a single tree-based algorithm. However, classification strategies employing several different algorithms in an ensemble setting to compensate for the limitations of any singly classification method are increasingly used in the exploitation of satellite images. Future research should therefore consider the adoption of an ensemble approach for river ice classification. Given the documented success achieved with decision-tree analysis, a logical extension would be the use of random forests to improve robustness and reduce errors.

Previous research on satellite-based river ice classification has demonstrated improved classification accuracy for region-based approaches over pixel-based methods. Accordingly, future research should consider evaluating the contribution of region-based classification strategies.

Acknowledgements

Funding for this research was provided through the Canadian Space Agency's Government Related Initiatives Program (GRIP). RADARSAT-2 imagery and IceBC output were made available by Natural Resources Canada. Aerial imagery and ice observation reports for training and validation was contributed by Alberta Environment and Parks.

References

Beltaos, S, and BC Burrell. 2015. Hydroclimatic Aspects of Ice Jam Flooding near Perth-Andover, New Brunswick. Canadian Journal of Civil Engineering 42 (9): 686–95.

Biggs, David, Barry De Ville, and Ed Suen. 1991. A Method of Choosing Multiway Partitions for Classification and Decision Trees. Journal of Applied Statistics 18 (1): 49–62.

Breiman, Leo, Jerome Friedman, Charles J Stone, and Richard A Olshen. 1984. Classification and Regression Trees. CRC press.

C-CORE. 2012. Operational Protocol for Satellite-Based River Ice Monitoring. Report R-09-054-720 Revision 2. C-CORE.

Chang, Li-Yen, and Wen-Chieh Chen. 2005. Data Mining of Tree-Based Models to Analyze Freeway Accident Frequency. Journal of Safety Research 36 (4): 365–75.

Chen, D, and Douglas Stow. 2002. The Effect of Training Strategies on Supervised Classification at Different Spatial Resolutions. Photogrammetric Engineering and Remote Sensing 68 (11): 1155–62.

Congalton, Russell G, and Kass Green. 1993. A Practical Look at the Sources of Confusion in Error Matrix Generation. Photogrammetric Engineering and Remote Sensing 59 (5): 641–44.

Costanza, Michael C, and Fred Paccaud. 2004. Binary Classification of Dyslipidemia from the Waist-to-Hip Ratio and Body Mass Index: A Comparison of Linear, Logistic, and CART Models. BMC Medical Research Methodology 4 (1): 1.

Deschamps, A, J van der Sanden, G Choma, JS Proulx-Bourque, and S Lemay. 2015. Operational Monitoring of River Ice Break-up Conditions Using RADARSAT-2 Images. Presented at the 36th Canadian Symposium on Remote Sensing, St. John, NL, Canada, June 8.

Dymond, John R, and Paul G Luckman. 1994. Direct Induction of Compact Rule-Based Classifiers for Resource Mapping. International Journal of Geographical Information Systems 8 (4): 357–67.

Fabricius, C, and K Coetzee. 1992. Geographic Information Systems and Artificial Intelligence for Predicting the Presence or Absence of Mountain Reedbuck. South African Journal of Wildlife Research 22 (3): 80–86.

Gauthier, Yves, Frank Weber, Stéphane Savary, Martin Jasek, Lisa-Marie Paquet, and Monique Bernier. 2006. A Combined Classification Scheme to Characterise River Ice from SAR Data. EARSeL eProceedings 5 (1): 77–88.

Gauthier, Y, Tremblay, M., Bernier, M. And C. Furgal, 2010. Adaptation of a Radar-Based River Ice Mapping Technology to the Nunavik Context. Canadian Journal of Remote Sensing, 36: (S1), 168-185.

Gauthier, Y., Hardy, St., Gutiérrez, C., Padel, A., Gaudreau, J., Poulin, J., Jasek, M., Bernier, M., Gomez, H. and Roth, A. 2015. IceFRONT: Integration of Radar and Optical Images for Operational River Freeze-Up Monitoring. In: Proceedings of the 18th Workshop on the Hydraulics of Ice Covered Rivers. Quebec City, QC, Canada: Canadian Geophysical Union - Hydrology Section, Committee on River Ice Processes and the Environment.

Gherboudj, I., Bernier, M. and Leconte, R. 2010. A Backscatter Modeling for River Ice: Analysis and Numerical Results. IEEE Transactions on Geoscience and Remote Sensing, Vol. 48, No. 4, 1788-1798.

Government of Canada, Environment and Climate Change Canada. 2009. Environment and Climate Change Canada - Water - Floods - Causes. March 30. https://www.ec.gc.ca/eau-water/default.asp?lang=En&n=E7EF8E56-1.

Jasek, M., Gauthier, Y., Poulin, J., & Bernier, M., 2013. Monitoring of Freeze-up on the Peace River at the Vermilion Rapids using RADARSAT-2 SAR data. In: Proceedings of the 17th Workshop on the Hydraulics of Ice Covered Rivers, Edmonton, AB, Canada: Canadian Geophysical Union - Hydrology Section, Committee on River Ice Processes and the Environment.

Haralick, Robert M, and Karthikeyan Shanmugam. 1973. Textural Features for Image Classification. IEEE Transactions on Systems, Man, and Cybernetics, no. 6: 610–21.

Kass, Gordon V. 1980. An Exploratory Technique for Investigating Large Quantities of Categorical Data. Applied Statistics, 119–27.

Khan, Amir Ali, and Thomas Puestow. 2010. Satellite-Based River Ice Monitoring for Flood Forecasting, River Flow Management and Climate Change Adaptation. presented at the ESA Living Planet Symposium, Bergen, Norway, July 28.

Khan, Amir Ali, and Thomas Puestow. 2015. Augmenting River Ice Flood Forecasting Services Using Satellite Radar Imagery. presented at the 36th Canadian Symposium on Remote Sensing, St. John's, NL, Canada, June 8.

Lees, Brian G, and Kim Ritman. 1991. Decision-Tree and Rule-Induction Approach to Integration of Remotely Sensed and GIS Data in Mapping Vegetation in Disturbed or Hilly Environments. Environmental Management 15 (6): 823–31.

Lopes, Armand, E Nezry, R Touzi, and H Laur. 1993. Structure Detection and Statistical Adaptive Speckle Filtering in SAR Images. International Journal of Remote Sensing 14 (9): 1735–58.

MDA. 2016. RADARSAT-2 Product Format Definition. RN-SP-52-1238 Issue 1/13. MacDonald, Dettwiler and Associates Ltd., Richmond, BC, Canada.

Mermoz, S., Allain, S., Bernier, M., Pottier, E. and Gherboudj, I. 2009. Classification of River Ice Using Polarimetric SAR Data. Canadian Journal of Remote Sensing 35 (5): 460-473.

Morgan, James N, and John A Sonquist. 1963. Problems in the Analysis of Survey Data, and a Proposal. Journal of the American Statistical Association 58 (302): 415–34.

Pelletier, KD, FE Hicks, and J van der Sanden. 2003. Monitoring Breakup on the Athabasca River Using RADARSAT-1 SAR Imagery. In: Proceedings of the 12th Workshop on the Hydraulics of Ice Covered Rivers. Edmonton, AB, Canada: Canadian Geophysical Union - Hydrology Section, Committee on River Ice Processes and the Environment.

Pelletier, KD, J van der Sanden, and FE Hicks. 2005. Synthetic Aperture Radar: Current Capabilities and Limitations for River Ice Monitoring. In Proceedings of the 17th Canadian Hydrotechnical Conference, Edmonton, Alberta, 1–10.

Pryse-Phillips, A, R Woolgar, K Rogers, M Lynch, T Puestow, and C Randell. 2009. Ice Observations on the Churchill River Using Satellite Imagery. In: Proceedings of the 15th Workshop on the Hydraulics of Ice Covered Rivers. St. John's, NL, Canada: Canadian Geophysical Union - Hydrology Section, Committee on River Ice Processes and the Environment.

Puestow, Thomas, Charles Randell, Ken Rollings, Amir Ali Khan, and Robert Picco. 2004. Near Real-Time Monitoring of River Ice in Support of Flood Forecasting in Eastern Canada: Towards the Integration of Earth Observation Technology in Flood Hazard Mitigation. In Geoscience and Remote Sensing Symposium, 2004. IGARSS'04. Proceedings. 2004 IEEE International, 4:2268–71. IEEE.

Quinlan, John Ross, Paul J Compton, KA Horn, and Leslie Lazarus. 1987. Inductive Knowledge Acquisition: A Case Study. In Proceedings of the Second Australian Conference on Applications of Expert Systems, 137–56. Addison-Wesley Longman Publishing Co., Inc.

Russell, Karen, Sherry Warren, Carl Howell, Thomas Puestow, Charles Randell, Amir Ali Khan, C. Mahabir, P. Tang, D. Burakov, and N. Novik. 2009. Improved Satellite-Based River Ice Monitoring Using Dual-Polarized SAR Imagery. CGU HS Committee on River Ice Processes and the Environment. In: Proceedings of the 15th Workshop on the Hydraulics of Ice Covered Rivers. St. John's, NL, Canada: Canadian Geophysical Union - Hydrology Section, Committee on River Ice Processes and the Environment.

Soh, L-K, and Costas Tsatsoulis. 1999. Texture Analysis of SAR Sea Ice Imagery Using Gray Level Co-Occurrence Matrices. IEEE Transactions on Geoscience and Remote Sensing 37 (2): 780–95.

Therneau, Terry M, and Elizabeth J Atkinson. 2015. Mayo Foundation, 2015: An Introduction to Recursive Partitioning Using the RPART Routines. Rstudio documentation.

Thistlethwaite, Jason, and Blair Feltmate. 2013. Assessing the Viability of Overland Flood Insurance: The Canadian Residential Property Market.

Tracy, Brian T, and Steven F Daly. 2003. River Ice Delineation with RADARSAT SAR. In: Proceedings of the 12th Workshop on the Hydraulics of Ice Covered Rivers. Edmonton, AB, Canada: Canadian Geophysical Union - Hydrology Section, Committee on River Ice Processes and the Environment.

Unterschultz, K. D., van der Sanden, J. and Hicks, F. E. 2009. Potential of RADARSAT-1 for the monitoring of river ice: Results of a case study on the Athabasca River at Fort McMurray, Canada. Cold Regions Science and Technology 55, 238–248.

van der Sanden, J, and A Deschamps. 2014. RADARSAT for River Ice Breakup Monitoring. Saint-Hubert, QC, Canada, November 19. ftp://ftp.cits.nrcan.gc.ca/pub/production/grip/kick_off_2014_11_19/RiverIce_GRIP_kick_of_Nov2014.pdf.

Weber, Frank, Dan Nixon, and Jeff Hurley. 2003. Semi-Automated Classification of River Ice Types on the Peace River Using RADARSAT-1 Synthetic Aperture Radar (SAR) Imagery. Canadian Journal of Civil Engineering 30 (1): 11–27.

Williams, Graham J. 2009. Rattle: A Data Mining GUI for R. The R Journal 1 (2): 45–55.